Journal of Sound and Vibration 329 (2010) 3798–3812

Contents lists available at ScienceDirect

Journal of Sound and Vibration

journal homepage: www.elsevier.com/locate/jsvi

PIV and LDV evidence of hydrodynamic instability over a liner in a duct with flow

David Marx [a,*], Yves Aurégan [b], Hélène Bailliet [a], Jean-Christophe Valière [a]

[a] Laboratoire d'Etudes Aérodynamiques (LEA), Université de Poitiers, ENSMA, CNRS, Bât. K, 40 Avenue du Recteur Pineau, 86 022 Poitiers Cedex, France
[b] Laboratoire d'Acoustique de l'Université du Maine (LAUM), Avenue Olivier Messiaen, 72085 Le Mans Cedex 9, France

ARTICLE INFO

Article history:
Received 20 October 2009
Received in revised form
19 March 2010
Accepted 22 March 2010
Handling Editor: D. Juve
Available online 18 April 2010

ABSTRACT

The acoustical behavior and the flow in a rectangular lined channel with grazing flow have been investigated. The liner consists of a ceramic structure of parallel square channels and is locally reacting. In the absence of flow, the liner has a classical behavior: the acoustic transmission coefficient has a minimum at the resonance frequency of the resonators. When the Mach number of the grazing flow increases, the material behavior becomes unclassical in the sense that its acoustic transmission increases strongly around the resonance frequency. To connect this behavior with flow features, the flow itself in the vicinity of a liner has been measured by means of laser velocimetry. Periodic structures have been observed along the liner that are phase-locked with the incident sound wave. The axial and transverse velocity of these structures bear the typical features of an instability. In particular, the wavelength, convection speed, and growth rate are given. This is the first time that an aeroacoustic instability resulting from the interaction of flow and sound over a liner is measured.

1. Introduction

Lined ducts are widely used to reduce noise radiation from ducts, from air conditioning systems to turbofan engines. In the presence of flow, acoustic propagation is difficult to predict due to noise/flow interaction. This is especially true in the vicinity of the lined wall where the flow is highly vortical. One feature of this interaction are nonlinear effects, which have an effect on peak absorption frequency and on sound transmission when the Mach number increases [1]. Another possible effect, which is the subject of the present paper, is the presence of an instability over the liner, which will decrease its performance if energy contained in the flow is passed towards acoustics.

An early evidence of sound amplification by a liner was obtained by Meyer et al. [2]. They observed sound amplification in a rectangular duct lined with Helmholtz resonators at sufficiently high flow speeds. The amplification was suppressed by adding a resistive face-sheet to the resonators. Unusually large sound transmission coefficients have also been measured by Brandes and Ronneberger [3] in cylindrical ducts lined with radial quarter-wavelength resonators. The sound was amplified for high flow speed, at a frequency close to the resonance frequency of the resonators. Recent measurements by Aurégan and Leroux [4] show an equivalent phenomenon, in a rectangular duct with a different type of liner, made of tightly packed square resonators. The common point between the afore-mentioned liners is their low resistance R (in any

* Corresponding author. Tel.: +33 5 49 45 39 72; fax: +33 5 49 45 36 63.
E-mail addresses: david.marx@lea.univ-poitiers.fr (D. Marx), yves.auregan@univ-lemans.fr (Y. Aurégan), helene.bailliet@lea.univ-poitiers.fr (H. Bailliet), jean-christophe.valiere@lea.univ-poitiers.fr (J.-C. Valière).

0022-460X/$ - see front matter © 2010 Elsevier Ltd. All rights reserved.
doi:10.1016/j.jsv.2010.03.025

case, $R/\rho_0 c_0 \leq 0.2$); also the incident sound wave was in all cases a plane wave. Sound amplification is a clear indication of the presence of an aeroacoustic instability.

Giving a detailed explanation to the instability resulting from the coupling between the flow and the liner proves to be a difficult task, partly due to the simplifications required during the analysis. A first insight has been given by Tester [5], who showed that with a mean plug flow, the response of a lined duct to an impulse contains some modes that are amplified during their propagation. This instability was found to be of the convective type. In the course of the analysis, the effect of the vorticity sheet on the wall impedance needs to be taken into account. A usual assumption is that the particle displacement is continuous across the vorticity sheet [6]: this leads to the classical model by Myers [7]. Other models are possible [8]. Tester [5] used the impedance model by Myers [7]. This model of the boundary conditions, together with the plug flow assumption, are widely used for the analytical prediction of sound propagation in ducts. Several recent analytical classifications of aeroacoustic modes rely on this model [9,10]. In his classification, Rienstra [9], besides acoustic modes, also predicts some unstable hydrodynamic modes. Though, the effect of the Myers boundary conditions has been questioned [5,11,12]. Vilenski and Rienstra [11] have avoided this model, and preferred to use instead an hyperbolic mean flow profile with zero velocity at the wall, making unnecessary the use of the Myers boundary condition. The actual impedance of the liner can then be used directly at the wall. The spatial analysis predicts that there are unstable modes, which tend to disappear when the ratio $\omega\delta/c_0$ falls below 0.1, where δ is the thickness of the hyperbolic tangent mean profile.

The propagation of sound in ducts has also been studied numerically, and some works mention instabilities that are not of a numerical nature. Li et al. [13] have computed the sound propagation in a lined duct with a Mach number of about 0.3 and compared their results to benchmark data by Jones et al. [15]. They used the linearized Euler equations and a time domain impedance boundary condition. They observed at 1 kHz an instability with some effect on sound transmission. The 1 kHz frequency at which the instability appears corresponds to a low liner resistance [14,15] (with $R/\rho_0 c_0 \sim 0.5$). Of course the use of Euler equations does not allow to conclude about the instability in a real flow including viscous effects. They nevertheless postulated that the instability would be of the Tollmien-Schlichting kind (they used a parabolic velocity profile) and that it would be reinforced because its natural frequency coincides with the resonance frequency of the liner. Burak et al. [14] have computed the flow and sound propagation in a lined duct with a Mach number of about 0.3 in the same configuration. Using a compressible large eddy simulation solver or a linearized Navier–Stokes solver, they also predicted at 1 kHz an instability pattern, but this was the case only when viscous effects in the vicinity of the lined wall were correctly taken into account. Sound transmission prediction by their code at the same 1 kHz frequency was correct only when the instability was well predicted. Although both Li et al. and Burak et al. observe an instability at 1 kHz under the same conditions, the physical mechanism remains unclear, since Li et al. observe the instability without any viscosity, while Burak et al. observe it only when viscous effects are taken into account sufficiently close to the wall.

As evidenced in the short review above, there is no clear-cut knowledge about the presence of an instability over a liner with mean flow. A difficulty, both for the analytical and numerical tools, is the reliability of the models they use. And unfortunately, there are few benchmark data against which the models can be compared with. Surprisingly, the existing experimental evidence [2–4] has dealt mainly with sound transmission coefficient measurements, from which an instability was inferred. But the flow itself in the vicinity of a liner displaying an instability has never been studied. A first attempt has been performed recently by Marx et al. [16] using particle image velocimetry (PIV). The measurements did show a probable instability but the result had to be analyzed in terms of proper orthogonal decomposition (POD) modes, no phase-locking of the measurement being done, and the flow was measured over only a part of the whole liner surface. In the present paper, laser velocimetry measurements of the flow along a lined wall of a channel are performed, with phase-locking on the acoustic excitation. The experimental setup is presented in Section 2, which includes a description of the rig and of the laser velocimetry. Results on the acoustic transmission coefficient are presented in Section 3, showing a singular behavior in agreement with the literature [2–4]. Finally, the outcome of laser flow measurements are presented in Section 4. An hydrodynamic instability is identified, and its main characteristics are given.

2. Experimental setup

2.1. Flow rig and experimental conditions

Top and side views of the flow rig are shown in Fig. 1. The rig is a pipe with a rectangular cross-section and is connected to a fan through a rubber-made vibrations absorber. The first part of the rig downstream of the fan has a 0.08 m × 0.03 m cross-section. A loudspeaker is mounted on that part and is driven in the frequency range 300 Hz–1.5 kHz. In this range only a plane acoustic wave can propagate, and the sound pressure level (SPL) is up to 145 dB. A 0.20 m long convergent is then used to reduce the rig cross-section from 0.08 m × 0.03 m down to 0.08 m × 0.02 m; this is in order to achieve a higher maximal velocity. The 0.60 m long test section has a rectangular cross-section 0.08 m × 0.02 m. We note H = 0.01 m the half channel height. Hence, the aspect ratio is 4, which was chosen as large as possible (to approach two dimensional flow conditions) without limiting the maximal velocity achieved with the fan. The test section is made of aluminum but has some glass windows for optical access. One of the walls is acoustically treated with a liner. The test section and the lining material are shown in Fig. 2. The liner is of the same type as the one used by Aurégan and Leroux [4], except for the

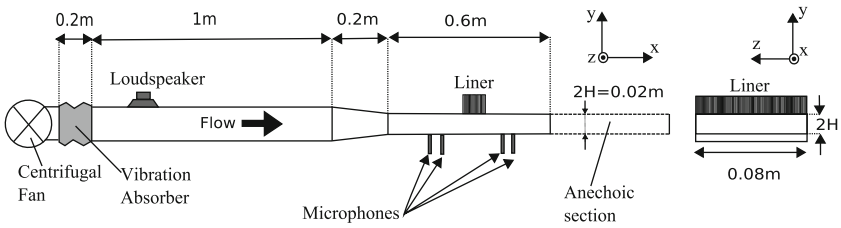

Fig. 1. Top and side views of the flow rig. Scales are different in *x*- and *y*-directions.

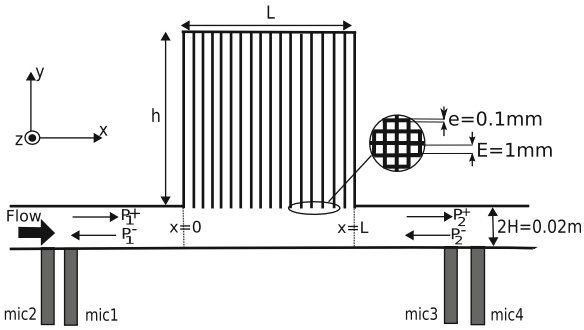

Fig. 2. Top view of the test section. The cross-section is rectangular, of height $2H=0.02$ m along the *y*-direction, and of width 0.08 m along the *z*-direction. The position of the microphones is: $x_{mic1}=-0.10$ m, $x_{mic2}=-0.185$ m, $x_{mic3}=0.23$ m, $x_{mic4}=0.315$ m.

resonance frequency which is slightly different. It consists of (quarter-wavelength) square ceramic resonators and comes from automotive industry (catalytic converters). The side of the resonators is $E=10^{-3}$ m. The resonators are separated by walls of thickness $e=10^{-4}$ m. The length of the resonators is $h=0.08$ m. The liner impedance (with no flow) can be estimated from relation (5) given by Aurégan and Leroux [4]:

$$\frac{Z}{\rho_0 c_0} = \frac{-\mathrm{i}}{Q}\cot(A\omega - \mathrm{i}\varepsilon/2), \tag{1}$$

where the time convention is $e^{i\omega t}$. This model of impedance is of the enhanced Helmholtz resonator type. In particular, the term ε accounts for the dissipation in the square channels and its value is: $\varepsilon=0.37$. The porosity is $Q=0.8$. The parameter $A=2.5\times10^{-4}$ sets the resonance frequency at about 1 kHz. The resistance close to resonance is approximately: $R/\rho_0 c_0 \sim 0.2$, which represents a low value. The resonance frequency (without flow) is 1 kHz; hence, with no flow, the acoustic transmission coefficient is expected to fall off at this frequency.

The total length of the wall that is treated with the liner is $L=0.075$ m. Finally the rig is ended by an anechoic termination, with a coefficient of reflexion at 1 kHz ranging from 0.05 (for no flow) up to 0.2 (for the highest mean flow velocity).

An important parameter is the velocity of the flow. In the test section, the mean central velocity is up to 108 m s^{-1}, which corresponds to a bulk velocity of 98 m s^{-1} (see Section 4.1) and a Mach number $M=0.27$.

2.2. Acoustical measurements setup

Acoustic measurements are performed for the plane mode by means of the four microphones shown in Fig. 2, using a swept sine excitation. On each side of the lined section, the plane acoustic wave is decomposed into complex incident and reflected components, with amplitudes P_1^+ and P_1^- upstream of the liner, and P_2^+ and P_2^- downstream of the liner. These four quantities are measured using a classical two microphones measurement on each side of the liner [17]. One can thus calculate the acoustic transmission coefficient $T=P_2^+/P_1^+$.

2.3. Optical velocimetry setup

The flow velocity in the vicinity of the liner is measured using laser velocimetry. The main technique used in this paper is 2D particle image velocimetry (2D PIV). Some additional laser doppler velocimetry (LDV) measurements have been performed as well. Both techniques and their application to the present experiment are the subject of the following two sections.

2.3.1. PIV measurements

PIV consists in taking two images of particles seeded in the flow [18,19]. By correlating the two images one can deduce the displacement of the particles, and then the particle velocity by dividing the estimated displacement by the time lag between the two images. An advantage of this technique is that it is weakly intrusive. It also makes it possible to obtain a instantaneous velocity map over some region of the flow (as opposed to point measurements). The measuring configuration for the present case is shown in Fig. 3. The laser sheet is introduced perpendicularly to the liner, and the camera (1376×1040 pixels) takes images of particles in the PIV measurement area (see Fig. 3). This area is about 0.03 m long in the x-direction and 0.02 m high in the y-direction. It does not cover the whole liner length, and three different series of measurements need be done to obtain the flow field over the whole lined part of the duct. The procedure of stitching the three series together is valid as far as only phase-averaged or statistical quantities are of interest here (see below for the phase locking procedure). The spatial resolution in both x- and y-directions is $\Delta \sim 1.8 \times 10^{-4}$ m. Note that spurious reflexions of the laser sheet on the walls means that at least the first four measured points close to the walls can give large errors. Thus it is difficult to measure the flow within 0.001 m from the wall. The x-axis origin is taken at the beginning of the treated portion of the duct, as shown in Fig. 2. The y-axis origin is taken at the center of the channel. The lined wall is then at $y=0.01$ m and the smooth wall is at $y=-0.01$ m. To compare the flow in the vicinity of the lined and smooth walls, a better vertical ordinate is the distance to the wall y_w, that will be used instead of y when necessary. Hence,

$$y_w = |y - y(\text{nearby wall})|.$$

In a previous study [16] the measurements were done randomly and results had to be interpreted using POD modes. In configurations when an acoustic excitation is used, it is possible to use the signal fed to the loudspeaker as a phase reference, and in the present study the images capture is phased locked onto this signal. The acquisition is done at $N_p=10$ phases during the acoustic period, T_a, of excitation. That is, the times t_p for the acquisition are

$$t_p = \frac{(p-1)}{N_p} T_a, \quad p = 1 \ldots 10.$$

For each of the 10 phases, $N_i=100$ instantaneous flow fields are measured. In configurations when no acoustic excitation is used, $N_p \times N_i=1000$ images are acquired randomly, so that the total number of acquisitions is the same with and without acoustic excitation.

The measured instantaneous PIV velocity vectors are noted $\mathbf{u_i}(x, y, p)$. Index p is for the phase and index i is for the image number, with $1 \le p \le N_p$ and $1 \le i \le N_i$. $\mathbf{u_i}$ has components u_i and v_i along x- and y-directions.

By averaging all the instantaneous velocity vectors $\mathbf{u_i}(x, y, p)$ at all the phases, we obtain the time averaged velocity vector $\mathbf{U_{av}}(x, y)$, with components U_{av} and V_{av}, given by

$$\mathbf{U_{av}}(x,y) = \frac{1}{N_p}\frac{1}{N_i}\sum_{p=1}^{N_p}\sum_{i=1}^{N_i}\mathbf{u_i}(x,y,p). \tag{2}$$

For each phase p, it is also possible to define the phase-averaged velocity vector $\mathbf{U}(x, y, p)$, obtained by averaging the N_i instantaneous fields $\mathbf{u_i}(x, y, p)$ at that phase:

$$\mathbf{U}(x,y,p) = \frac{1}{N_i}\sum_{i=1}^{N_i}\mathbf{u_i}(x,y,p), \quad p = 1 \ldots 10. \tag{3}$$

This quantity is defined only for phase-locked data acquisition. It is useful to subtract the time average velocity to obtain the fluctuations at each phase:

$$\mathbf{u}(x,y,p) = \mathbf{U}(x,y,p) - \mathbf{U_{av}}(x,y), \tag{4}$$

with component $u(x, y, p)$ and $v(x, y, p)$.

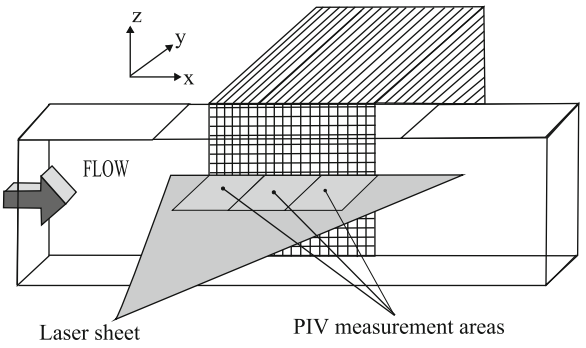

Fig. 3. PIV measurements setup. Three different measurement areas are used to cover the whole velocity field over the liner.

Another quantity of interest is the root mean square velocity vector, $\mathbf{u_{rms}}$, with components u_{rms} and v_{rms}. It is given by

$$\mathbf{u_{rms}}(x,y)=\sqrt{\frac{1}{N_p}\frac{1}{N_i}\sum_{p=1}^{N_p}\sum_{i=1}^{N_i}(\mathbf{u_i}(x,y,p)-\mathbf{U_{av}}(x,y))^2}. \tag{5}$$

This quantity is defined for phase-locked data acquisition, but an equivalent quantity can be defined for a random acquisition made without phase locking, simply by setting $N_p=1$ and $N_i=1000$ in the above formulas. Hence, the rms velocity is useful for comparing cases with and without phase locking, that is with or without acoustic excitation.

For reasons that will appear clear later, in case of acoustic excitation (phase-locked measurements) it will be interesting to extract from the phase-averaged velocity fluctuation only that part corresponding to the frequency of excitation, $f_a=1/T_a$. Let us consider $u(x, y, p)$ for example. Being T_a-periodic, $u(x, y, p)$ is a sum of harmonic contributions at multiples of f_a. To extract the fundamental component at f_a, we need to calculate the first term of the Fourier series at that frequency, $X_{u,a}(x, y)$. If u were continuously dependent on t, $X_{u,a}$ would be given by

$$X_{u,a}(x,y)=\frac{1}{T_a}\int_0^{T_a}u(x,y,t)\mathrm{e}^{-\mathrm{j}2\pi f_a t}\,\mathrm{d}t.$$

As u is discrete, the series is discretized, so that:

$$X_{u,a}(x,y)=\frac{1}{N_p}\sum_{p=1}^{N_p}u(x,y,p)\mathrm{e}^{-\mathrm{j}2\pi(p-1)/N_p}, \tag{6}$$

which is nothing but the discrete fourier transform of $u(x, y, p)$ divided by N_p. From the knowledge of $X_{u,a}(x, y)$, one obtains easily the phase $\phi_u(x,y)$ and amplitude $A_u(x, y)$ of $u(x, y, p)$ in the whole spatial domain considered. Similar quantities $X_{v,a}(x, y)$, $\phi_v(x,y)$, and $A_v(x, y)$ are defined for the transverse velocity fluctuation v.

2.3.2. LDV measurements

In addition to PIV measurements, some laser doppler velocimetry (LDV) [20,21] measurements have been performed. The principle of the method is to make two laser beams interfere, thus creating a pattern of fringes. A particle seeded in the flow, when going through the fringes, will scatter the light of the laser. The resulting burst is collected by a photomultiplier, and its frequency is related to the velocity of the particle. The velocity of the flow is thus measured at a particular point that can be moved in the fluid. Here, the velocity was measured in backscattering mode, the seeding being the same as with PIV, with mean data rates of at least 10 kHz. A total number of 10^5 samples of the velocity were acquired for each spatial position. Contrary to PIV measurements, no phase locking is used, even when there is an acoustic excitation.

One advantage of LDV over PIV is that time-resolved measurements are possible, and that more data are available for computing statistics such as the average and rms. LDV results will be used mainly for comparison with PIV results. Also, spurious reflexions are spoiling the PIV velocity fields located within 0.001 m from the lined wall, a problem that was not encountered in LDV measurements. Hence, LDV has been used to measure the flow close to the wall, at a distance down to $y_w=5\times10^{-4}$ m from the wall.

A result from a LDV measurement is a velocity time series of the form $u(x, y, t_i)$, where (x, y) is a selected position, and t_i, $i=1\ldots10^5$, are random times. The averaged velocity, phase-averaged velocity, and root mean square velocity, as defined by Eqs. (2), (3), and (5) in the section on PIV measurements, are defined in an equivalent manner for the LDV (with some caution due to the unevenly spaced data). So their definition is not repeated here. As for the PIV, it will be useful to extract the component of the velocity corresponding to the frequency of excitation. For this we have to calculate the Fourier transform of the signal at frequency f_a. This is given by

$$X_{u,a}(x,y)=\int_0^{\infty}u(x,y,t)\mathrm{e}^{-\mathrm{j}2\pi f_a t}\,\mathrm{d}t. \tag{7}$$

Since the velocity is only available at discrete times t_i, the integral has to be discretized. One also needs a phase reference and this is provided by the loudspeaker signal, to which the above equation is also applied. The knowledge of $X_{u,a}(x, y)$ gives once again access to the phase $\phi_u(x,y)$ (with reference to the loudspeaker phase) and to the amplitude $A_u(x, y)$ at selected positions (x, y).

3. Results for acoustic measurements

This section presents the result of the measurements of acoustic transmission by the liner for different mean flow Mach numbers. The frequency and amplitude of the incident plane acoustic wave are varied.

The modulus of the acoustic transmission coefficient, $|T|$, is given as a function of frequency in Fig. 4 for two different conditions: no flow ($M=0$), and a mean flow with Mach number $M=0.27$. Without flow the transmission is close to 0 for the resonance frequency of the liner which is around 1 kHz. At $M=0.27$, there is a hump in the transmission in the vicinity of this frequency, with a peak of about 0.5 at $f_a=1060$ Hz. This hump does not appear as long as $M<0.2$. It is shown for several values of the Mach number exceeding this value in Fig. 5. The resonance frequency as well as the transmission maximum increase with the Mach number. The maximum of the transmission does not increase linearly with the Mach number and

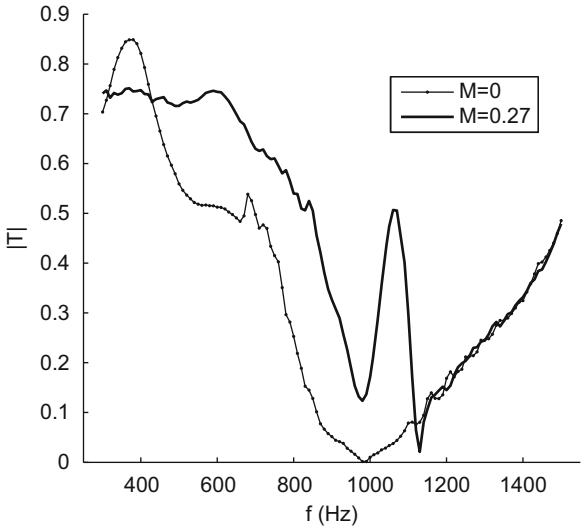

Fig. 4. Modulus of the acoustic transmission coefficient.

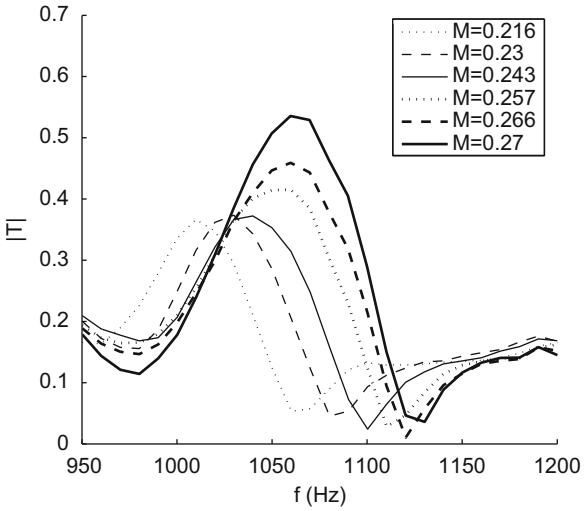

Fig. 5. Zoom on the peak in transmission for several Mach numbers.

varies more strongly between M=0.257 and 0.27. Parts of these changes (in particular the value of the frequency shift) are probably due to an increase of the temperature from an ambient value of 293 K with no flow to a value up to 306 K with flow at M=0.27 (due to fan heating), a temperature that would corresponds to a new resonance frequency with no flow of 1.1 kHz.

A hump in the transmission such as the one observed here has been reported before in two previous studies [3,4]. The transmission was up to three [4] for a liner equivalent to the present one but with a slightly different geometrical setup. It will be shown in the next section that this hump is connected to an underlying flow instability, and is triggered by the incident acoustic wave. One may thus expect a change in the transmission when the level of the excitation varies. To investigate whether this is the case or not, the variation of the transmission with frequency is measured for several values of the incident acoustic level, L_i, where $L_i = 20\log(P^+_{1,\,\mathrm{rms}}/0.00002)$. The incident level is varied by changing the input voltage to the loudspeaker, with a ratio of 1:16. The result is shown in Fig. 6. A slight shift in the peak frequency is observed, but the incident level has little effect indeed on the transmission peak. This means that somehow, the sound produced by the instability is proportional to the incident sound.

4. Results for flow measurements

The results of the previous section are a strong motivation to study the flow itself in the vicinity of the liner. Measurements of the flow velocity by laser velocimetry are now presented. In the remaining, only the maximal velocity

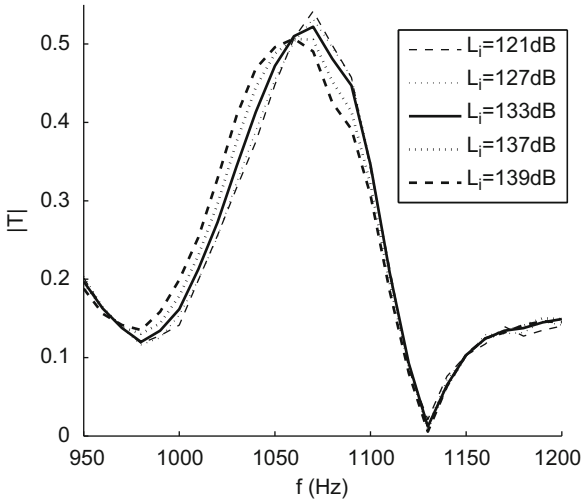

Fig. 6. Modulus of the acoustic transmission coefficient for several sound pressure levels L_i of the incident acoustic wave: M=0.27.

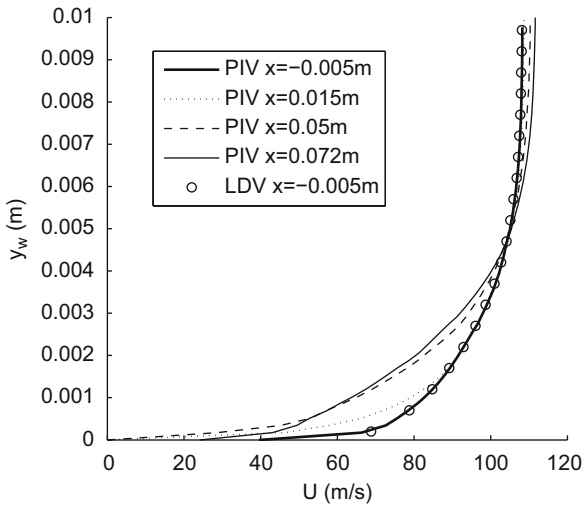

Fig. 7. Mean velocity profiles above the lined wall: M=0.27 and L_i=133 dB.

achievable with the present setup is considered, and details on the corresponding mean flow conditions are provided in Section 4.1. The response of the flow to an incident acoustic excitation is then studied in 4.2. The fixed excitation frequency, f_a=1060 Hz, coincides with the frequency of the hump observed in Section 3.

4.1. Mean flow

The centerline velocity upstream of the liner is $U_c \sim 108\,\mathrm{m\,s^{-1}}$. The corresponding bulk velocity is U_m=98 m s^{-1} (based on the cross-sectional average of the PIV time-averaged axial velocity), giving a Mach number of M=0.27. The corresponding Reynolds number is $\mathrm{Re} = HU_c/\nu = 72\,000$. Another useful number is the Reynolds in wall units that will be given below.

The mean velocity profiles just upstream from and above the liner are shown at several axial positions in Fig. 7, where an acoustic excitation at f_0=1060 Hz and L_i=133 dB is used. The agreement between PIV and LDV is then very good at $x = -0.005$ m, just upstream from the liner (this agreement is obtained after offsetting the LDV y-axis by -3×10^{-4} m; this is due to difficulties in locating the exact location of the wall using PIV. Even without this offset, the agreement is very correct). There is a strong axial evolution of the profiles and the liner is not long enough in the x-direction for the flow above it to be fully developed (even if profiles at $x \sim 0.05$ m and $x \sim 0.072$ m are not very different). The profiles are less steep above the liner than above the rigid wall upstream. This is equivalent to what happens during the transition from a rigid wall to a rough wall in a pipe [22].

At high Reynolds numbers like the one considered here, a logarithmic region is expected above a rigid wall, with a velocity given by [22]

$$U^+ = \frac{1}{\kappa}\ln(y_w^+) + B, \tag{8}$$

where $\kappa = 0.4$ and $B = 5.5$ are experimental constants. The + indicates that variables are made dimensionless using wall units, that is, the friction velocity u_τ and the distance $y_\tau = \nu/u_\tau$. The previous relation may be written equivalently in standard units:

$$U = \frac{u_\tau}{\kappa}\ln(y_w) + C. \tag{9}$$

The velocity profiles from Fig. 7 are plotted on semilog axes in Fig. 8, where the two vertical lines mark the region $0.1H < y_w < 0.2H$ where the relation (9) is expected to hold. The profile at $x = -0.005$ m upstream of the liner is linear in that region. A linear fit on the curve $(\ln(y_w), U)$ gives access to the value of $u_\tau/\kappa = 12.9$, and assuming the value given above for κ, we obtain: $u_\tau = 5.2\,\mathrm{m\,s^{-1}}$. This value is classically of the order of 4–5 percent of the centerline velocity [22], and it gives a wall units based Reynolds number $Re_\tau = Hu_\tau/\nu \sim 3400$.

The velocity profiles above the liner are also plotted on semilog axes in Fig. 8. A logarithmic region is not observed very clearly for these profiles (and there is no reason this should be so).

4.2. Fluctuating flow and instability

The acoustic excitation frequency $f_a = 1060$ Hz fed to the loudspeaker corresponds approximately to the maximal value for the sound transmission at $M = 0.27$ (see Fig. 6) and two levels of excitation are used, namely $L_i = 133$ and 139 dB.

4.2.1. General observations

Phase-averaged axial and transverse velocity fluctuations, as given by Eq. (4) are shown in Fig. 9 for four different phases. Only the upper half-channel is represented, the top wall at $y = 0.01$ m being the lined wall. Spatially periodic structures moving and growing in the direction of the flow are clearly seen along the lined wall. The effect of the level of excitation on the phase-averaged velocity is shown at one single phase in Fig. 10. The size and intensity of the structures increase with the excitation.

4.2.2. Transverse variations of rms velocity

As was mentioned in Section 2, root mean square velocities are convenient to compare cases with and without acoustic excitation, that is with and without phase-locking. The y-profiles of the total rms fluctuations are shown in Figs. 11 and 12. The axial position for these profiles is $x = 0.07$ m. In case of acoustic excitation structures are clearly seen at this position (see Fig. 9). The fluctuations are stronger along the lined wall than the rigid wall, and they are increased by an incident acoustic waves, in agreement with Fig. 10. The most visible effect seems to be on the transverse velocity v which is increased over the full cross-section of the fluid, and whose maximum is moving away from the wall when the excitation increases. Fig. 13 shows a comparison between PIV and LDV measurements, the latter being more precise because

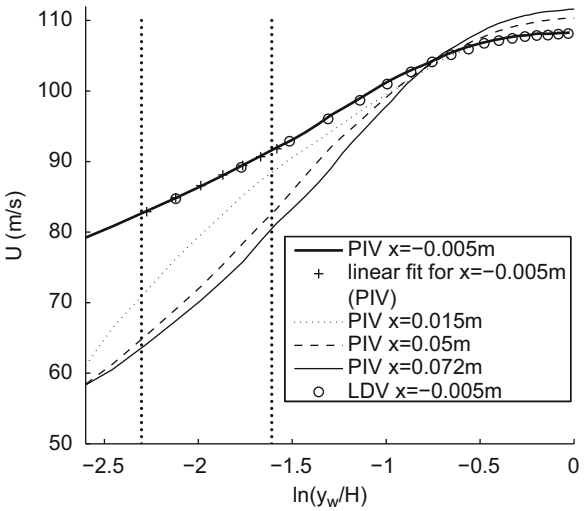

Fig. 8. Mean velocity profiles plotted in semilog axes. The two vertical lines correspond to the region $0.1H < y_w < 0.2H$ where a logarithmic layer is expected. The linear fit on the mean velocity upstream of the liner ($x = -0.0015$ m) in the logarithmic region is also shown.

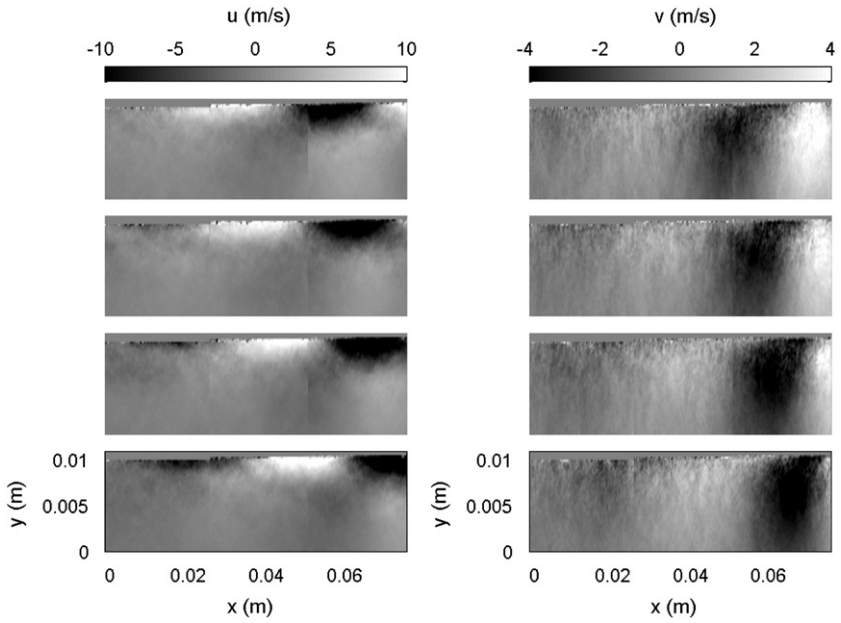

Fig. 9. Maps of the phase-averaged velocity over the top half of the channel, with the lined wall at y=0.01 m. Left: $u(x, y, p)$ and right: $v(x, y, p)$. Four consecutive phases are shown from top to bottom (p=1–4): M=0.27 and L_i= 133 dB.

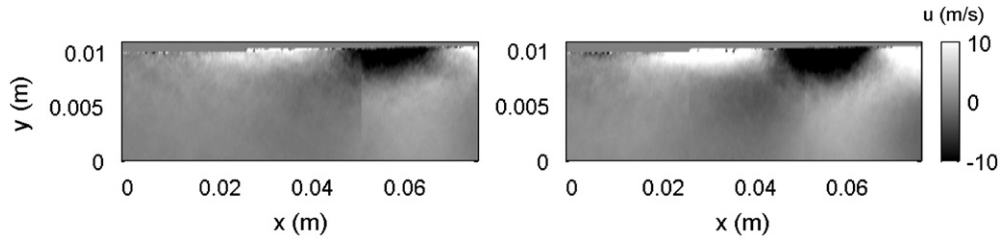

Fig. 10. Maps of the phase-averaged velocity over the top half of the channel, with the lined wall at y=0.01 m. Left: $u(x, y, p)$ at phase p=1 for L_i= 133 dB and right: $u(x, y, p)$ at phase p=1 for L_i= 139 dB: M=0.27.

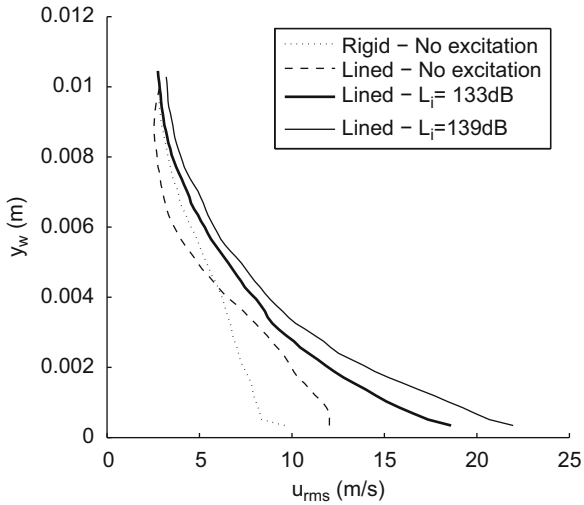

Fig. 11. Profiles of u_{rms} over the liner, at x=0.07 m, with or without excitation. The profile above a rigid wall is shown for reference.

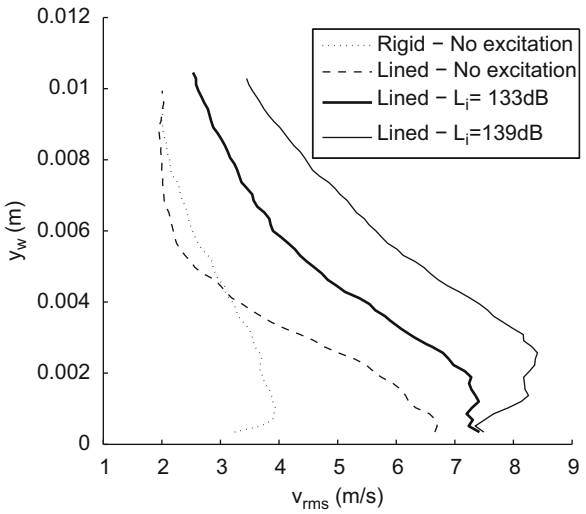

Fig. 12. Profiles of v_{rms} over the liner, at x=0.07 m, with or without excitation. The profile above a rigid wall is shown for reference.

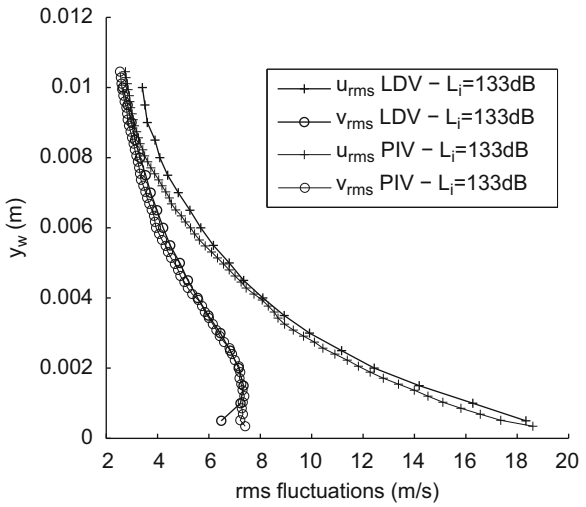

Fig. 13. Comparison between the rms profiles measured by PIV and LDV: x=0.07 m and L_i=133 dB.

calculated over much more data. The agreement is correct except at the center of the channel for u and close to the wall. As was explained above PIV is unable to give precise results close to the wall in the present configuration.

4.2.3. Instability wave

The rms velocity as shown in the previous section takes into account every velocity perturbation. Now it is desirable to extract only that part of the perturbation whose frequency corresponds to the acoustical excitation frequency, f_a. This extraction is performed via Fourier analysis as explained in Sections 2.3.1 and 2.3.2.

The PIV measurements are first analyzed this way. Recall for example that the transverse velocity fluctuation at frequency f_a may be written as

$$v_a(x,y,p) = \mathrm{Re}[X_{v,a}(x,y)\mathrm{e}^{\mathrm{i}(2\pi f_a t_p)}] = \mathrm{Re}[A_v(x,y)\mathrm{e}^{\mathrm{i}(2\pi f_a t + \phi_v(x,y))}], \quad p = 1 \ldots 10. \tag{10}$$

As an example, the phase for the transverse component is shown in Fig. 14 for the higher level of excitation. The phase is almost independent of y and is a linear function of x. This is better seen in Fig. 15 where the unwrapped phase is plotted at some fixed vertical position y_0=0.0075 m (that is, some fixed distance $y_{w,0}$=0.0025 m from the lined wall). The phase can thus be written approximately in the form:

$$\phi_v(x) = -k_r x. \tag{11}$$

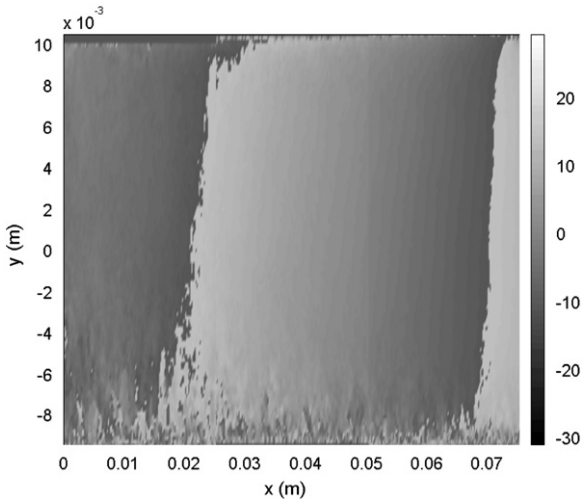

Fig. 14. Map of the phase $\phi_v(x,y)$ of the transverse velocity: L_i= 139 dB and M=0.27.

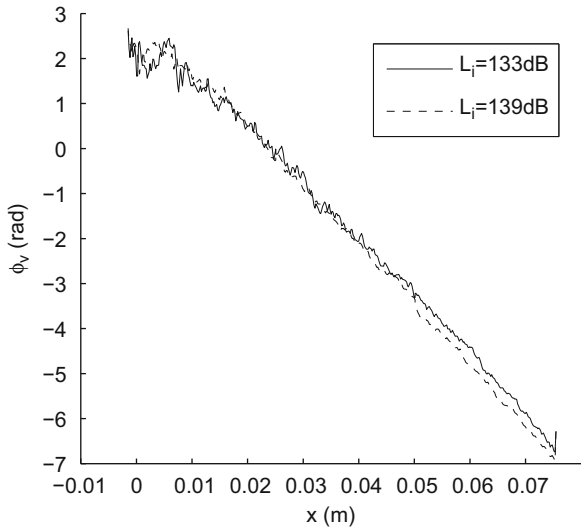

Fig. 15. Phase $\phi_v(x,y_0)$ of the transverse velocity at y_0=0.0075 m, for two levels of excitation: L_i=133 and 139 dB and M=0.27.

The slope $-k_r$ does not depend on the level of excitation, as seen in the figure. For the high level of excitation (L_i=139 dB) a linear fit gives $k_r \sim 130.6\,\mathrm{m}^{-1}$ (the phase is first averaged over y in the region $y_0 \pm 0.0009$ m and then the fit is performed on this average). The corresponding wave length is given by $\lambda = 2\pi/k_r \sim 0.048$ m, and the phase velocity is $c = 2\pi f_a/k_r \sim 51\,\mathrm{m\,s}^{-1}$. For the low level of excitation, results are very close: $k_r \sim 125.6\,\mathrm{m}^{-1}$, $\lambda \sim 0.05$ m, $c \sim 53\,\mathrm{m\,s}^{-1}$.

The amplitude $A_v(x, y)$ for the transverse velocity is shown in Fig. 16, it is seen to increase with x and this axial dependence is now analyzed further.

The amplitude $A_v(x, y_0)$ is plotted as a function of x in Fig. 17 for the levels of excitation; the considered vertical position y_0 is the same as above for the phase. The amplitude is well fitted by an exponential, as shown in the figure. The amplitude dependence on x is therefore of the form $e^{k_i x}$. The value of k_i does not depend much on the level of excitation. For L_i=139 dB, the fit provides the value $k_i \sim 29\,\mathrm{m}^{-1}$ (again, a y-average is performed prior to the fit). For L_i=133 dB, $k_i \sim 32.4\,\mathrm{m}^{-1}$.

Note from Fig. 17 that when the acoustic excitation is doubled (from 133 to 139 dB), the amplitude A_v is also roughly doubled. This was also apparent from Fig. 10. This behavior means that the unstable liner acts as an amplifier, which supports the idea that the instability is of the convective type.

Finally, the transverse variation of the amplitude is considered. For different axial positions, the ratio $A_v(x,y)/e^{k_i x}$ is computed and plotted in Fig. 18. The variation of this ratio with y does not depend on the chosen value of x. Hence, the amplitude may be written in its final form:

$$A_v(x,y) = \psi_v(y) e^{k_i x}$$

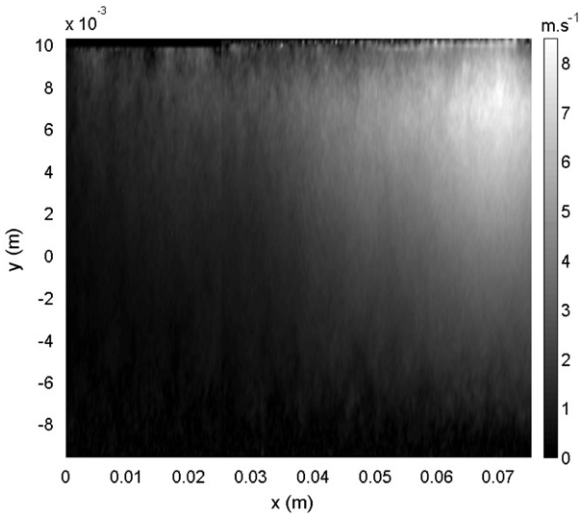

Fig. 16. Maps of the amplitude $A_v(x, y)$ of the transverse velocity: L_i=139 dB and M=0.27.

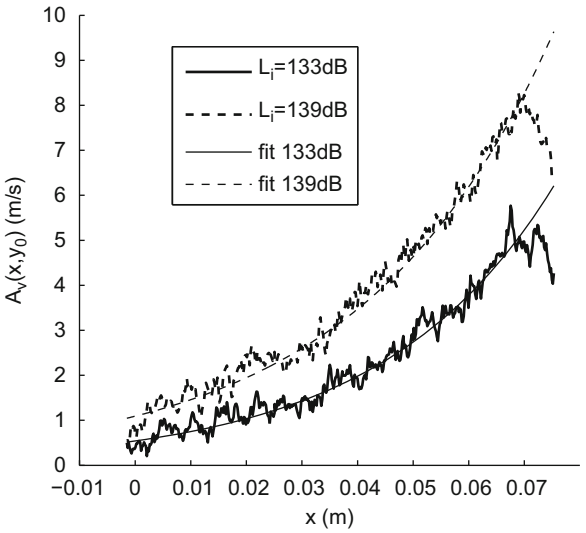

Fig. 17. Amplitude $A_v(x, y_0)$ of the transverse velocity at y_0=0.0075 m, for two levels of excitation: L_i=133 and 139 dB and M=0.27. Also represented are the exponential fits to the amplitude.

and the transverse velocity at the excitation frequency is

$$v_a(x,y,p) = \psi_v(y) e^{k_i x} e^{i(2\pi f_a t_p - k_r x)},$$

where $\psi_v(y)$ is an eigenfunction depending only on the transverse coordinate. The velocity can be interpreted as the result of an instability, with k_i a spatial growth rate. An equivalent form is found for the axial velocity. Both axial and transverse normalized eigenfunctions, obtained after averaging $A(x,y)/e^{k_i x}$ over x, are finally given in Fig. 19. These functions do not depend much on the level of excitation even if only those at the higher level are shown. At this point, the instability is fully characterized, since its wavelength, propagation speed, growth rate and shape (eigenfunction) are known.

A similar analysis can be conducted on the LDV measurements. In particular, measurements have been performed for the axial velocity u, at several axial positions at a distance y_w=0.001 m from the lined wall, for L_i=133 dB. At this distance from the wall, many PIV data are spoiled due to reflexions. The evolution of the amplitude $A_u(x, y_w=0.001)$ and phase $\phi_u(x,y_w = 0.001\,\text{m})$ given by a Fourier analysis are shown in Figs. 20 and 21. For $x > 0.015$ m, the phase is linear with x and the amplitude has an exponential-like dependence. A linear fit on the phase gives: k_r=121.8 m^{-1}, corresponding to a wavelength $\lambda = 0.051$ m, and a phase velocity: $c = 2\pi f_0/k_r = 56.7\,\text{m s}^{-1}$. An exponential fit on the phase gives $k_i \sim 29.6\,\text{m}^{-1}$. These value are in good agreement with the corresponding value obtained using PIV.

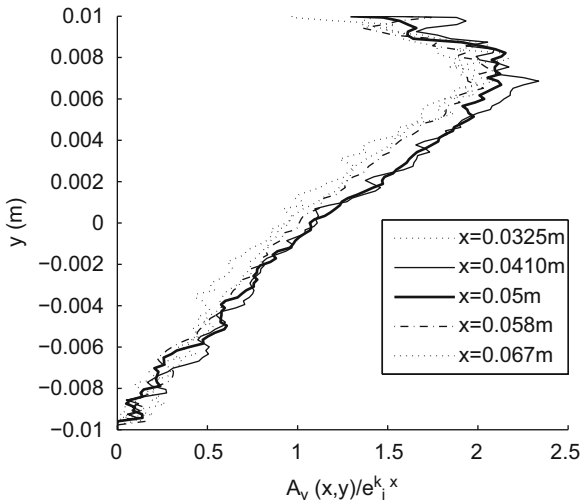

Fig. 18. Transverse profiles of $A_v(x,y)/e^{k_i x}$ for different values of the axial position, x: L_i=139 dB and M=0.27.

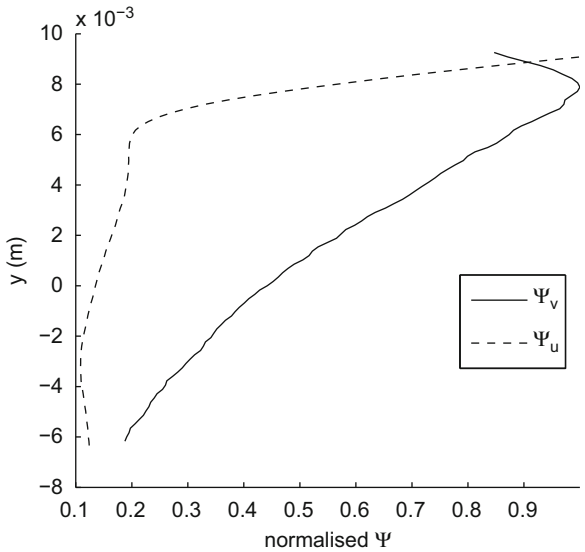

Fig. 19. Normalized eigenfunctions ψ_v and ψ_u: L_i=139 dB and M=0.27.

An interesting feature of the curve in Fig. 20 lies in the fact that what looks like another exponential behavior is observed in the region $x < 0.015$ m. Whether this part is the result of a stabilization zone past the rigid/lined transition, or whether it is a primary instability is not known. A close examination of some reflexion free PIV results confirms that the amplitude A_u in the region $x < 0.015$ m has an exponential growth with a growth rate of about 90–100 m^{-1}.

To conclude that part the relative amplitudes of the instability wave and of the background turbulence are assessed. The total fluctuations are given by the rms velocity (Eq. (5)). This can be split into a coherent part, and an uncoherent part:

$$v_{\mathrm{rms}}^2 = v_{\mathrm{rms,\ coh}}^2 + v_{\mathrm{rms,\ uncoh}}^2. \tag{12}$$

Here, "coherent" means correlated with the acoustic excitation (and thus with the instability), while "uncoherent" refers to all that turbulence that is not in the instability. Knowing the amplitude of the instability wave, an equivalent rms value for the coherent part is given by

$$v_{\mathrm{rms,\ coh}}(x,y) = A_v(x,y)/\sqrt{2}. \tag{13}$$

From v_{rms} and $v_{\mathrm{rms,\ coh}}$, it is possible to obtain $v_{\mathrm{rms,\ uncoh}}$ from Eq. (12). In Fig. 22 the different rms transverse velocities are given in the vicinity of the liner at an axial position x=0.07 m. The total rms is the same as in Fig. 12, and displays turbulence rates of about 8 percent. The coherent and incoherent parts have equivalent contributions (with the uncoherent part maximal at the lined wall and the coherent part maximal away from the wall). Quantitatively similar results are

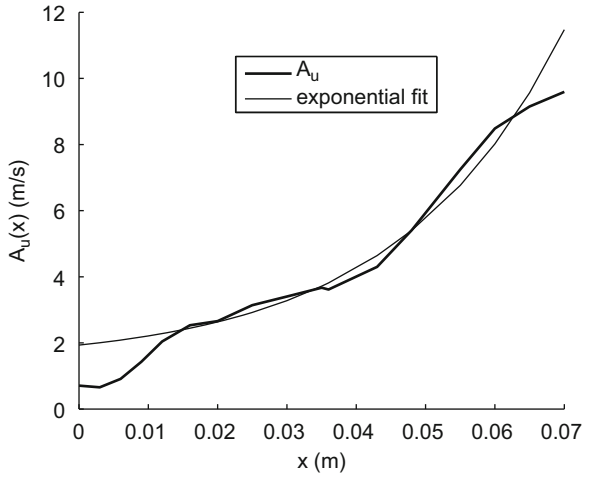

Fig. 20. Axial evolution of the amplitude $A_u(x, y_w=0.001\,\text{m})$ as measured by LDV: $L_i=133\,\text{dB}$ and $M=0.27$.

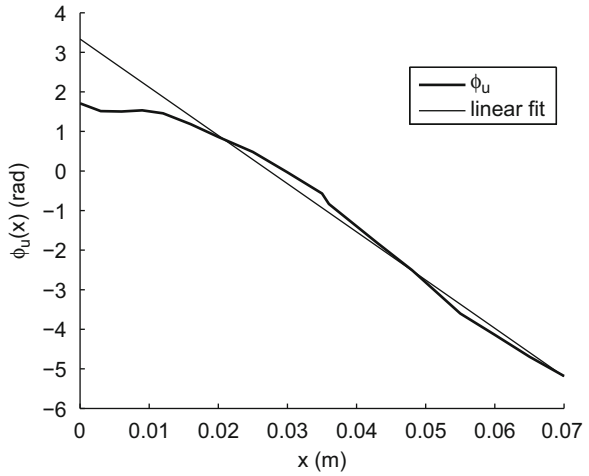

Fig. 21. Axial evolution of the phase $\phi_u(x,y_w=0.001\,\text{m})$ as measured by LDV: $L_i=133\,\text{dB}$ and $M=0.27$.

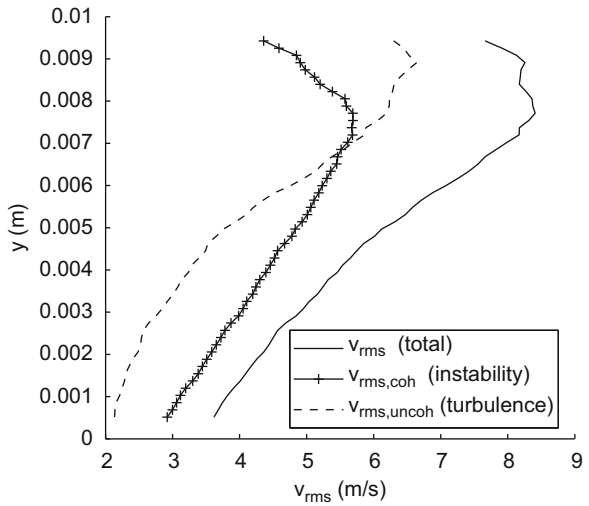

Fig. 22. Profiles of v_{rms} over the liner, at $x=0.07\,\text{m}$. The total rms is as defined by Eq. (5). The coherent part (the instability) is given by Eq. (13), and the uncoherent part is obtained from Eq. (12): $L_i=139\,\text{dB}$ and $M=0.27$.

obtained for the axial velocity. More details are given in [23], where the coherent and uncoherent parts were calculated in a different way, but with similar results.

5. Conclusion

The experimental study reported here shows the presence of an instability over the liner and its effect on sound transmission in realistic conditions: a Mach number of 0.27, an upstream Reynolds of about 70 000 (corresponding to a value of 3400 in wall units). The acoustic liner is made of quarter-wavelength resonators with a resonance frequency of 1 kHz, and a low resistance $R/\rho_0 c_0 \sim 0.2$. In the presence of an incident sound wave at the resonance frequency, the flow is unstable over the liner. Some characteristics of the instability have been established: the wavelength is about 0.05 m, the phase speed is about $53\,\mathrm{m\,s^{-1}}$ (approximately the half centerline velocity of the flow), and the growth rate is about $29\,\mathrm{m^{-1}}$. The transverse eigenfunctions for both the axial and transverse components of the velocity have been given. The axial velocity peaks very close to the wall, while the transverse velocity peaks farther away from the wall.

Due to the sudden transition from a rigid wall to a lined wall, the mean velocity profiles over the liner strongly depends on the axial position. An axial evolution is also observed for the fluctuating velocity behavior for which two consecutive regions of exponential growth have been distinguished (first region for $x < 0.015$ m, close enough to the wall and second region for $x > 0.015$ m), even if more evidence are still needed in the first region. The first region may be a sort of mixing region resulting from the transition from a rigid to a lined wall, or it may consist in a primary instability. Accordingly, the instability in the second region, characteristics of which have been given, would corresponds to a primary instability or to a secondary one. More work is required in the future to fully characterize that first region.

References

[1] Y. Aurégan, M. Leroux, V. Pagneux, Measurement of liner impedance with flow by an inverse method, *Proceedings of the 10th AIAA/CEAS Aeroacoustics Conference*, Manchester, UK, AIAA Paper 2004-2838, 2004.
[2] E. Meyer, F. Mechel, G. Kurtze, Experiments on the influence of flow on sound attenuation in absorbing ducts, *Journal of the Acoustical Society of America* 30 (1958) 165–174.
[3] M. Brandes, D. Ronneberger, Sound amplification in flow ducts lined with a periodic sequence of resonators, *Proceedings of the First AIAA/CEAS Aeroacoustics Conference*, Munich, Germany, AIAA Paper 95-126, 1995.
[4] Y. Aurégan, M. Leroux, Experimental evidence of an instability along an impedance wall with flow, *Journal of Sound and Vibration* 317 (2008) 432–439.
[5] B.J. Tester, The propagation and attenuation of sound in lined ducts containing uniform or plug flow, *Journal of Sound and Vibration* 28 (1973) 151–203.
[6] U. Ingard, Influence of fluid motion past a plane boundary on sound reflection, absorption, and transmission, *Journal of the Acoustical Society of America* 31 (1959) 1035–1036.
[7] M.K. Myers, On the acoustic boundary condition in the presence of flow, *Journal of Fluid Mechanics* 71 (1980) 429–434.
[8] Y. Aurégan, R. Starobinski, V. Pagneux, Influence of grazing flow and dissipation effects on the acoustic boundary conditions at a lined wall, *Journal of the Acoustical Society of America* 109 (2001) 59–64.
[9] S.W. Rienstra, A classification of duct modes based on surface waves, *Wave Motion* 37 (2003) 119–135.
[10] E.J. Brambley, N. Peake, Classification of aeroacoustically relevant surface modes in cylindrical lined ducts, *Wave Motion* 43 (2006) 301–310.
[11] S. Rienstra, G. Vilenski, Spatial instability of boundary layer along impedance wall, *Proceedings of the 14th AIAA/CEAS Aeroacoustics Conference*, Vancouver, Canada, AIAA Paper 2008-2932, 2008.
[12] E.J. Brambley, Fundamental problems with the model of uniform flow over acoustic linings, *Journal of Sound and Vibration* 322 (2009) 1026–1037.
[13] X. Li, C. Richter, F. Thiele, Time-domain impedance boundary conditions for surfaces with subsonic mean flows, *Journal of the Acoustical Society of America* 119 (2006) 2665–2676.
[14] M.O. Burak, M. Billson, L.-E. Eriksson, S. Baralon, Validation of a time and frequency domain grazing flow acoustic liner model, *Proceedings of the 14th AIAA/CEAS Aeroacoustics Conference*, Vancouver, Canada, AIAA Paper 2008-2929, 2008.
[15] M.G. Jones, W.R. Watson, T.L. Parrott, Benchmark data for evaluation of aeroacoustic propagation codes with grazing flow, *Proceedings of the 11th AIAA/CEAS Aeroacoustics Conference*, Monterey, California, AIAA Paper 2005-2853, 2005.
[16] D. Marx, Y. Aurégan, H. Bailliet, J.C. Valière, Sound amplification in a lined duct with flow: PIV measurements, *Proceedings of the Euronoise Conference*, Paris, France, 2008.
[17] P.O.A.L. Davies, Practical flow duct acoustics, *Journal of Sound and Vibration* 124 (1988) 91–115.
[18] R.J. Adrian, Particle Imaging technique for experimental fluid mechanics, *Annual Review of Fluid Mechanics* 23 (1991) 261–304.
[19] D. Marx, H. Bailliet, J.-C. Valière, Analysis of the acoustic flow at the abrupt change of section in an acoustic waveguide using PIV and POD, *Acta Acustica United with Acustica* 94 (2008) 54–65.
[20] P. Buchhave, W.K. George, J.L. Lumley, The measurement of turbulence with the LASER-doppler anemometer, *Annual Review of Fluid Mechanics* 11 (1979) 443–503.
[21] A. Minotti, F. Simon, Gantié, Characterization of an acoustic liner by means of laser doppler velocimetry in a subsonic flow, *Aerospace Science and Technology* 12 (2008) 398–407.
[22] H. Schlichting, *Boundary-Layer Theory*, seventh ed., McGraw-Hill, New York, 1979 (See Chapter XX).
[23] D. Marx, Y. Aurégan, H. Bailliet, J.C. Valière, Evidence of hydrodynamic instability over a liner in a duct with flow, *15th AIAA/CEAS Aeroacoustics Conference*, Miami, Florida, USA, AIAA Paper 2009-3170, 2009.